HHS Public Access

Author manuscript

Acta Biomater. Author manuscript; available in PMC 2024 March 23.

Published in final edited form as:

Acta Biomater. 2022 January 15; 138: 453–462. doi:10.1016/j.actbio.2021.10.048.

Synergistic interventional photothermal therapy and immunotherapy using an iron oxide nanoplatform for the treatment of pancreatic cancer

Meng Wang[a], **Yong Li**[c], **Miao Wang**[b], **Kaili Liu**[d], **Ashley R. Hoover**[d], **Min Li**[e], **Rheal A Towner**[f], **Priyabrata Mukherjee**[g], **Feifan Zhou**[b,*], **Junle Qu**[a,*], **Wei R Chen**[d,*]

[a]Key Laboratory of Optoelectronic Devices and Systems of Ministry of Education and Guangdong Province, College of Physics and Optoelectronic Engineering, Shenzhen University, Shenzhen 518060, China

[b]School of Biomedical Engineering, Hainan University, Haikou 570228, China

[c]Interventional Therapy Department, Tianjin Key Laboratory of Cancer Prevention and Therapy, Tianjin Medical University Cancer Institute and Hospital, Tianjin 300060, China

[d]Stephenson School of Biomedical Engineering, University of Oklahoma, Norman, OK 73019, USA

[e]Department of Medicine, Department of Surgery, University of Oklahoma Health Sciences Center, Oklahoma City, OK, USA

[f]Advanced Magnetic Resonance Center, Oklahoma Medical Research Foundation, Oklahoma City, OK, USA

[g]Department of Pathology, University of Oklahoma Health Sciences Center, Oklahoma City, OK, USA

Abstract

Pancreatic cancer (PC) is the most lethal malignancy due to its high metastatic ability and poor drug permeability. Here, a synergized interventional photothermal-immunotherapy strategy was developed with imaging guidance and temperature monitoring by magnetic resonance imaging (MRI) technique, for the local treatment of metastatic PC. A tumor microenvironment (TME)-responsive nanoplatform was fabricated via coating of DSPE-PEG and indocyanine green

*Corresponding authors. zhouff@hainanu.edu.cn (F. Zhou), jlqu@szu.edu.cn (J. Qu), Wei-R-hen@ou.edu (W.R. Chen).

Declaration of Competing Interest

The authors declare that they have no known competing financial interests or personal relationships that could have appeared to influence the work reported in this paper.

CRediT authorship contribution statement

Meng Wang: Investigation, Formal analysis, Writing – original draft, Writing – review & editing. **Yong Li:** Investigation, Formal analysis, Writing – review & editing. **Miao Wang:** Conceptualization. **Kaili Liu:** Investigation, Formal analysis, Writing – review & editing. **Ashley R. Hoover:** Investigation, Formal analysis, Writing – review & editing. **Rheal A Towner:** Software, Writing – review & editing. **Priyabrata Mukherjee:** Funding acquisition, Writing – review & editing. **Feifan Zhou:** Conceptualization, Investigation, Formal analysis, Writing – original draft, Writing – review & editing. **Junle Qu:** Writing – original draft, Writing – review & editing. **Wei R Chen:** Conceptualization, Supervision, Writing – original draft, Writing – review & editing.

Supplementary materials

Supplementary material associated with this article can be found, in the online version, at doi:10.1016/j.actbio.2021.10.048.

(ICG) onto imiquimod (IMQ) loaded amorphous iron oxide nanoparticles (IONs). This unique nanoplatform, IMQ@IONs/ICG, served as a contrast agent for MRI, a drug delivery vehicle for IMQ and ICG, and a catalyst for TME modulation. The biodegradable IMQ@IONs/ICG was also non-toxic, and improved the penetration of the loaded drugs in PC to maximize thermal ablation of the tumor and minimize damage to the surrounding healthy tissue. For the treatment of aggressive, metastatic Panc02-H7 pancreatic tumors in mice, ION-assisted MRI was employed to guide the administration of interventional photothermal therapy (IPTT) and monitor the temperature distribution in target tumor and surrounding tissue during treatment. The local IPTT treatment induced *in situ* immunogenic cell death (ICD), and, in combination with released IMQ, triggered a strong antitumor immunity, leading to decreased metastases and increased CD8+ in spleen and tumors. With precise local treatment and monitoring, treated primary tumors were completely eradicated, mesentery metastases were dramatically reduced, and the survival time was significantly prolonged, without damage to normal tissue and systemic autoimmunity. Overall, this synergistic strategy represents a promising approach to treat PC with significant potential for clinical applications.

Keywords

Amorphous iron oxide nanoparticle; Pancreatic cancer; Magnetic resonance temperature imaging; Interventional photothermal therapy; Immunotherapy

1. Introduction

Pancreatic cancer (PC) remains the most lethal malignancy worldwide with a dismal 9% 5-year survival rate for patients of all stages [1,2]. Especially, over 50% of patients have distal metastases at diagnosis, with only 3% 5-year survival rate [3]. In clinical practice, surgery and radiotherapy are the standard choices to remove or control the primary tumors in PC patients. However, clinical results are unsatisfactory due to the low resectability of PC tumors in patients and their high recurrence rates [4]. Recently, photodynamic therapy, sonodynamic therapy, and radiotherapy have been developed for precise control of local tumors, with the advantages of less pain, minimal invasion, and improved curative effect [5-9]. However, little progress has been made in controlling tumor metastasis. Due to the limited diagnostic ability, poor prognosis, and rapid metastasis of PC, it is paramount to develop better therapeutic strategies to control both primary tumors and metastases.

Immunotherapy is considered the best choice for controlling metastases by triggering systemic immune responses to identify, destroy, and remove residual tumor cells [10,11]. However, immunotherapy alone cannot be used to completely remove large solid tumors without inducing high toxicity to the whole body [12,13]. Recently, phototherapy-synergized cancer immunotherapies have been developed for solid metastatic tumors, combining phototherapy with immunoadjuvants, CAR-T therapy, and immunological checkpoint inhibitors [14-16]. Some combination strategies have been utilized for the treatment of advanced melanoma, metastatic breast cancer, and neck and head tumors [17,18]. Recently, various nanoplatforms have been developed for phototherapy-synergized cancer immunotherapy [19-25]. Benefitting from the modifiable structure and versatile

functions of nanomaterials, great progress has been made in phototherapy-synergized cancer immunotherapy for solid tumors [26-28]. Nanomaterials as multi drug carriers can enhance the dispersion or stability of photosensitizers or immunoadjuvants, reduce the side effects and improve the therapeutic efficacy [29,30]. In addition, these nanomaterials have unique physicochemical properties. As a result, they not only have excellent photothermal properties, but can also remodel the immune-suppressive environment of solid tumors [31,32]. Until now, most studies have focused on the construction of nanomaterials with high efficiency for killing cancer cells, or improving the tumor targeting ability and drug delivery capacity of nanomaterials. However, the poor tissue penetration depth of light severely limits the effectiveness of these combination strategies for deeply seated tumors. Imaging guided loco-regional interventional photothermal therapy (IPTT) was developed to address the challenges of light penetration for PTT, especially for PC patients with deep-buried tumors in the abdomen [6,7,33,34]. Under the imaging guidance, this treatment modality not only accurately destroyed the primary tumor, but also avoided the damage of normal tissues. Therefore, rational combination of IPTT with immunotherapy is very promising as an efficient PC therapy.

The real-time monitoring of temperature distribution in deep tumors is critical for IPTT treatment. Temperature gradient created by IPTT in the target tissue can affect the immunogenicity and lethality of tumor cells, which in turn can determine the therapeutic outcome. Magnetic resonance imaging (MRI) has been widely employed for noninvasive diagnosis and treatment guidance with high spatial resolution [35,36]. Moreover, MRI can accurately monitor the spatial temperature distribution in the target tissue in real-time using water proton resonance frequency (PRF) method [37-44]. The PRF method possesses the advantages of high sensitivity, excellent linearity with temperature, and tissue non-dependency. Thus, combining MRI technique with IPTT-synergized immunotherapy to monitor and guide the therapeutic process of PC is highly desirable.

Magnetic nanoparticles made of pure metals, metal oxides, and magnetic nanocomposites are widely used as MRI contrast agents in preclinical and clinical settings [45-47]. Among them, iron oxide nanoparticles (IONs) are the most popular due to their excellent biocompatibility [48,49]. IONs have been proved to modulate the tumor microenvironment (TME) by converting type 2 macrophages into type 1 macrophages [50]. Also, iron ions derived from IONs can accelerate Fenton-like reaction and cause accumulation of ROS in TME, leading to efficient tumor inhibition [51,52]. Moreover, IONs as MRI agents have been well investigated in MR temperature imaging [53]. As a poorly permeable tumor, PC resists various type of drug delivery [54,55]. In the poorly permeable pancreatic tumor model, 30 nm polymeric micelles have much better tumor penetration than 100 nm polymeric micelles [56]. However, small nanoparticles (<5.5 nm) can be quickly eliminated by the renal system with low accumulation in targeting tissue. Therefore, designing multiple functional IONs with desirable size can enhance drug delivery, and, when combined with other therapies, could significantly improve the efficacy in treating PCs.

Herein, an IPTT-synergized immunotherapy was developed, with MR imaging guidance and real-time temperature monitoring, using amorphous iron oxide nanoparticles (IONs) loaded with imiquimod (IMQ) as an immunoadjuvant, and indocyanine green (ICG) as a

photothermal agent. This synergistic strategy, using the unique nanoplatform, IMQ@IONs/ICG, provides the following specific advantages: (1) improves penetration in PC with a reasonable nanocarrier size of 37.5 nm; (2) acts as a contrast agent for MRI, a drug carrier for IMQ and ICG, and a catalyst for TME modulation; (3) enables accurate, real-time monitoring of temperature changes in PCs and the peritumoral normal tissue during treatment, maximizing thermal ablation effect of the tumor and minimizing damage to the healthy tissue; (4) leads to elimination of primary tumors and induces antitumor immunity against metastases and tumor recurrence, by *in situ* vaccination and TME modulation. The schematic of the IMQ@IONs/ICG-mediated IPTT-synergized immunotherapy for the treatment of metastatic pancreatic tumors is given in Scheme 1.

2. Experimental

2.1. Preparation of IMQ@IONs

Imiquimod filled iron oxide nanoparticles were prepared via a modified microemulsion approach [57]. Briefly, a water-in-oil microemulsion was prepared by dissolving 1.82 g CTAB, and 5 mL 1-hexanol in 50 mL of n-dodecane. A mixture of 1 mg imiquimod, 1500 μL H_2 O and 500 μL methanol was added to this micellar system. After equilibration and formation of a transparent microemulsion, 100 μL of concentrated H_2 O_2 was added and 2 mL of $Fe(CO)_5$ was injected in a few seconds. After a short homogenization period (5–10 s), the stirrer was switched off. Twelve hours later, 10 mL of DEG was added to the microemulsion, which initiated phase separation. The DEG bottom phase contained the nanoscale solid. Thereafter, the product was purified by two cycles of centrifugation and resuspension in ethanol.

2.2. Preparation of IMQ@IONs/ICG

Imiquimod-encapsulated IONs (IMQ@IONs) were dispersed in ethanol (4 mg mL^{-1}), followed by mixing with ICG at concentration of 1 mg mL^{-1}. Then, the mixture was slowly added into an aqueous solution of DSPE-PEG_{2K} (5 mg mL^{-1}), and stirred for 10 min. Finally, the resulting nanoparticles (IMQ@IONs/ICG) were purified by three cycles of centrifugation and resuspension in purified water, and then re-dispersed in PBS.

2.3. Pancreatic carcinoma mouse model

C57BL/6 mice (six to eight weeks) were purchased from Harlan Sprague Dawley Co. and housed in the animal facility of the Department of Comparative Medicine at the University of Oklahoma Health Sciences Center (OUHSC, Oklahoma, OK). All animal procedures were performed in accordance with the Guidelines for Care and Use of Laboratory Animals published by the US National Institutes of Health (NIH) and approved by the University of Oklahoma Health Sciences Center (OUHSC) Institutional Animal Care and Use Committee (IACUC). An orthotopic model of pancreatic cancer was established using a surgical procedure [58,59]. Briefly, Panc02-H7 cells (5×10^4 in 50 mL medium) were injected into the pancreatic tails of C57BL/6 mice. The animals were ready for experiments in approximately 7 to 10 days when the pancreatic tumors reached a size of 8 mm (approximately 300 mm^3) in diameter.

2.4. Photothermal therapy study in the pancreatic carcinoma mouse model

Tumor bearing mice were randomly assigned to five different groups ($n = 8$) and PBS, ICG, IONs, and IMQ@IONs/ICG were respectively injected into the mice via the tail vein. Two hours after injection, mice were anaesthetized with 2% v/v isoflurane, and an optical fiber (Pioneer Optics) with a cylindrical active lens (10 mm) was inserted into the center of the tumor through an 18-gauge percutaneous transhepatic cholangiography needle. The tumor was irradiated by the laser with a power of 1 W and a duration of 10 min. The surface temperature was recorded by infrared thermal imaging camera, and the temperature distribution in the tumor was recorded on a 7.1 Tesla MR scanner (Bruker Biospin, USA). The calibration of MRT measurement of temperature distribution in target tissue during laser irradiation has been performed in the previous studies using gel phantoms, *ex vivo* tissue, chicken breast tissue, and animal tumors, by comparing the results from MRT and interstitial thermocouple measurements [60-62].

2.5. Antitumor immunity study in pancreatic carcinoma mouse model

To observe the antitumor effects, treated mice were sacrificed on day 7 and the tumors and blood were harvested to analyze the immune cell distribution and cytokine production. Tumor tissues were isolated, minced, and digested with Collagenase IV (1 mg mL^{-1}) and DNase I (20 μg mL^{-1}) at 37 °C for 30 min in RPMI. Cells were filtered through nylon mesh filters and washed with PBS. The single-cell suspension was incubated with anti-CD16/32 to reduce nonspecific binding to Fc receptors. To analyze the active T cells, cells were stained with the following antitumor fluorescent anti-bodies: Live/Dead-Zombie 405, CD45-eFluor 450, CD3-APC-eFluor 780, CD8a- FITC, CD4-PE-CY7, CD25-APC, and Foxp3-PE. To analyze Tumor-associated macrophages (TAM), cells were stained with Live/Dead-Zombie 405, CD45-eFluor 450, CD11b-PE, F4/80-APC, CD206-FITC. A Stratedigm S1200Ex flow cytometer (Stratedigm, USA) was used for flow cytometry, and data analysis was conducted using FlowJo software. Serum was isolated from blood and diluted prior to analysis. Interleukin 6, interleukin 12, and interleukin 10 were analyzed via enzyme-linked immune sorbent assay (ELISA) kits (R&D Systems, USA) according to the manufacturer's protocol. The representative flow cytometry plots and corresponding gating strategies are given in Figs. S22 to S28.

2.6. Statistical analysis

Values are expressed as mean ± standard error of the mean. The data were analyzed using GraphPad Prism software (GraphPad Software Inc., La Jolla, CA, USA).

3. Results and discussion

3.1. Characteristics of biodegradable IMQ@IONs/ICG nanoparticles

IMQ@IONs/ICG nanoparticles were constructed with a stepwise method. First, IMQ@IONs were prepared *via* a reverse microemulsion approach [57]. Transmission electron microscopy (TEM) image showed that IMQ@IONs were monodispersed with a uniform size of ~19.2 ± 4.3 nm in diameter (Fig. 1A). The successful loading of IMQ in IMQ@IONs was confirmed by FT-IR and TGA analyses (Figs. S1 and S2), and the loading

capacity of IMQ was ≈ 83%, as measured using a UV–vis–NIR spectrophotometer. Then, IMQ@IONs were loaded with ICG *via* hydrophobic interaction, and coated with a PEG shell to avoid agglomeration. Dynamic light scattering (DLS) analysis confirmed the size of IMQ@IONs/ICG nanoparticles with an average diameter of 37.5 nm (Fig. 1B), and the loading capacity of ICG was ≈ 62 %, as confirmed by Vis-NIR spectra (Figs. 1C and S3). IMQ@IONs/ICG nanoparticles also showed excellent long-term stability after immersion in serum for 7 days (Fig. S4). T_2-weighted MR signals determined the magnetic relaxation of MQ@IONs/ICG, which showed a dose-dependent darkening effect, with R_2 value of 0.993 (Fig. 1D).

IMQ@IONs/ICG nanoparticles could be decomposed in a slightly acidic environment (Fig. S5), which could be used for the release of iron ions and accelerated Fenton-like reaction to produce •OH. As shown in Fig. S6, the electron spin resonance (ESR) amplitude of DEPMPO-OH was significantly increased at pH 6.8, compared to that at pH 7.4, suggesting that IMQ@IONs/ICG nanoparticles improved the production of •OH at acidic conditions. Moreover, the nanoparticle decomposition led to fast IMQ release (Fig. S7). The photothermal effect of IMQ@IONs/ICG was confirmed by the dramatic increase in temperature in ICG and IMQ@IONs/ICG solutions under 805 nm laser irradiation (Figs. 1E and S8). Cycle heating experiment confirmed that the photo-stability of ICG loaded on the nanoparticles was significantly improved, compared to ICG alone (Fig. 1F). The photothermal conversion efficiency of IMQ@IONs/ICG was calculated to be 37.3%. These results indicated that IMQ@IONs/ICG nanoparticles were biodegradable and retained the properties of both IONs and ICG.

3.2. Effects of IMQ@IONs/ICG on tumor cells and immune cells

The intracellular uptake behavior of IMQ@IONs/ICG was investigated in Panc02-H7 cells. Confocal laser scanning microscope (CLSM) analysis demonstrated the colocalization of IMQ@IONs/ICG with lysosomes (Figs. 2A and S9), through endocytosis of the nanoparticles. The fluorescence signals of Panc02-H7 cells incubated with IMQ@IONs/ICG were remarkably higher than those of cells incubated with free ICG, demonstrating the efficient uptake of IMQ@IONs/ICG (Fig. S10).

IMQ@IONs/ICG nanoparticles can decompose at acidic pH, which can contribute to the release of iron ions and accelerate Fenton-like reaction producing •OH. To determine •OH production in tumor cells by IMQ@IONs/ICG, a cellular fluorescence probe of •OH, aminophenyl fluorescein (APF), was employed (Fig. 2B). Compared with the control and ICG groups, Panc02-H7 cells in IONs and IMQ@IONs/ICG groups showed stronger fluorescence signal of •OH, indicating the generation of •OH from the conversion of endogenous intracellular H_2O_2 *via* Fenton-like reaction.

The phototoxicity of IMQ@IONs/ICG towards Panc02-H7 cells was determined using CCK-8 assay and apoptosis assay. Panc02-H7 cells maintained good viability after being cocultured with IMQ@IONs/ICG at different concentrations for 24 h, but showed a high-level of cell death when irradiated by an 805 nm laser (Fig. S11). The *in vitro* phototoxicity of IMQ@IONs/ICG was further evaluated by Annexin V-FITC/PI staining and Calcein-AM/PI staining. As shown in Fig. 2C,D, the ICG-alone or ION-alone only

provided limited photothermal effect under the irradiation of the laser light. However, when ICG is conjugated with ION, the photothermal effect increased significantly, demonstrating the synergistic effects of IONs and ICG for cellular uptake and photothermal cytotoxicity. All these data indicated that IMQ@IONs/ICG could be used as a good biocompatible nanoplatform for PTT.

PTT can elicit immunogenic cell death (ICD) by causing dying tumor cells to release damage associated molecular patterns (DAMPs), which can induce an adaptive antitumor immune response. Therefore, two kinds of crucial DAMPs, calreticulin (CRT) and HMGB1, were further investigated. CRT exposure on the surface of Panc02-H7 cells was evaluated by immunofluorescence and flow cytometry. IMQ@IONs/ICG + L induced a much higher level of CRT exposure on cell surface, compared with the treatment by ICG + L (Figs. 2E; S12 and 13). The production and release of HMGB1 from Panc02-H7 cells were determined by immunofluorescence and ELISA analyses. IMQ@IONs/ICG + L significantly increased HMGB1 production and release (Figs. S14 and S15). These results demonstrated that IMQ@IONs/ICG-mediated PTT could induce ICD.

Dendritic cells (DCs) are a key type of antigen-presenting cells (APCs), which are responsible for activating native T cells. Next, the maturation of bone marrow-derived dendritic cells (BMDCs) induced by IMQ@IONs/ICG was investigated. As shown in Fig. 2F and G, IMQ@IONs/ICG triggered a higher-level expression of CD80 and CD86 on the surface of DCs compared to ICG and IONs/ICG treatments, indicating maturation of BMDCs stimulated by IMQ. Furthermore, the enhanced secretion of tumor necrosis factor α (TNF-α) by DCs was observed under the treatment of IMQ@IONs/ICG (Fig. S16). Overall, all these results indicated the efficient uptake of IMQ@IONs/ICG by tumor cells to trigger •OH generation *via* Fenton-like reaction, which further enhanced the phototoxicity by laser irradiation, creating *in-situ* ICD to achieve antitumor immunity. In addition, IMQ@IONs/ICG acted as a nanoadjuvant to cause DC maturation, which in turn enhanced the ICD initiated antitumor immunity.

3.3. *Therapeutic effects of IMQ@IONs/ICG* in vivo

To determine the *in vivo* effects of IMQ@IONs/ICG, orthotopic pancreatic tumor-bearing mice were used. The *in vivo* biodistribution of IMQ@IONs/ICG was analyzed by multimodal imaging (Fig. 3 A). As shown in Fig. S17, the ICG fluorescence signal of IMQ@IONs/ICG group was remarkably stronger than that of ICG group. The ICG fluorescence signal of ICG group indicated the highest tumor accumulation within 1 h and then gradually metabolized and cleared from the circulating blood, while the fluorescence signal of ICG in IMQ@IONs/ICG group indicated long-term circulation. The ex vivo fluorescence imaging also confirmed the significantly high accumulation of IMQ@IONs/ICG in tumor tissue 24 h after injection (Fig. S17). These data indicated that IMQ@IONs/ICG avoided rapid elimination by systemic circulation and enhanced the tumor accumulation. In addition, IMQ@IONs/ICG showed the highest accumulation in tumors at 3 h, providing an optimal treatment time for interventional PTT. Then, the *in vivo* biodistribution of IMQ@IONs/ICG was further studied by T_2-weighted MR imaging. Strong MR signal was detected in the tumor after injection of IMQ@IONs/ICG,

which increased gradually over time within 3 h (Fig. 3 B). The signal changes in tumors or surrounding tissues at different time points were further quantified based on the time-dependent T_2 relaxation times. From the results of the T_2 values of tumors, it was evident that IMQ@IONs/ICG gradually accumulated in tumor tissue and reached the highest level at 3 h post injection (Fig. S18), consistent with the results of fluorescence imaging (Fig. S17). Hematology and blood biochemistry analysis and H&E staining of the main organs of mice demonstrated no visible toxicity induced by the nanoparticles (Figs. S19 and S20). The pharmacokinetics of IMQ@FNPs/ICG was further studied, and the half-life of IMQ@FNPs/ICG blood circulation was estimated to be ~ 41.2 min (Fig. S21). These results confirmed that IMQ@IONs/ICG could be safely employed as an MR/fluorescence imaging contrast agent for interventional PTT guidance.

The therapeutic effects were then investigated with Panc02-H7 orthotopic tumor model under the guidance of MR imaging (Fig. 3A). Mice were intravenously administered with IMQ@IONs/ICG, ICG, or PBS, about 7–10 days after tumor cell inoculation in pancreas when the tumor reached a size of 300 mm^3. The laser fiber was inserted into the tumor by a hollow percutaneous transhepatic cholangiography needle under MR imaging guidance at 3 h post injection (Fig. S22). The temperature distribution in tumor was monitored during the interstitial PTT by PRF-shift MR thermometry. As shown in Fig. 3C, the heating effect diffused rapidly around the NIR fiber, and then was stable after 3 min irradiation. In the IMQ@IONs/ICG group, the maximum temperature in the tumor was increased by 35 °C within 3 min. However, the surrounding healthy tissues did not exhibit significant temperature increase during the treatment, as shown in Fig. 3C. Thus, the high tumor-specific enrichment of IMQ@IONs/ICG not only improved the photothermal efficiency, but also reduced the damage to healthy tissues. The temperature changes in tumor were further evaluated by an infrared thermal imager during interstitial PTT. Thermal images showed that the temperature of tumors in IMQ@IONs/ICG + L group was much higher than that in ICG + L group (Fig. S23). The photothermal effect was further studied *via* staining sections of harvested tumors one day after treatment. H&E and TUNEL staining showed that tumor structures were severely damaged in the IMQ@IONs/ICG + L group (Fig. 3F). These results confirmed that IMQ@IONs/ICG plus laser treatment provided excellent tumor killing effects.

On the basis of the photothermal effect induced by IMQ@IONs/ICG based interventional PTT, its synergistic photo-immunotherapeutic effects *in vivo* were next investigated. Mice bearing Panc02-H7 orthotopic tumors were divided into five treatment groups: PBS, PBS + L, IMQ@IONs/ICG, IONs/ICG + L and IMQ@IONs/ICG + L. Mice were sacrificed 7 days post administration to analyze the synergistic efficiency of the treatment. The tumor volumes in IONs/ICG + L and IMQ@IONs/ICG + L groups were smaller compared to that in the control group (Fig. 4A). In addition, IMQ@IONs/ICG based interventional PTT significantly reduced the metastases. In fact, there were almost no mesenteric metastases 7 days after treatment (Fig. 4B and C). The therapeutic efficacy of IMQ@IONs/ICG + L also translated into improved average survival time of the tumor-bearing mice (Fig. 4D). The median survival times of mice in the PBS, PBS + L, IMQ@IONs/ICG, IONs/ICG + L and IMQ@IONs/ICG + L groups were 31, 30, 33, 40, and 56 days, respectively. These results

confirmed that IMQ@IONs/ICG based interventional PTT was highly effective for slowing the pancreatic tumor growth and inhibiting metastasis.

3.4. Antitumor immune responses induced by IMQ@IONs/ICG

To further understand the antitumor immune response triggered by IMQ@IONs/ICG based interventional PTT-immunotherapy, the tumor infiltrations of TAMs, T lymphocytes and immunosuppressive regulatory T cells (T_{regs}) were investigated. As shown in Fig. 5A, the populations of M2-like TAMs showed an obvious reduction in IMQ@IONs/ICG, IONs/ICG + L, and IMQ@IONs/ICG + L groups, which can be ascribed to the polarization of TAM to the M1-like phenotype by iron oxide nanoparticles. This polarization was further confirmed by the reduced level of IL-10 and the increased level of interleukin-12 (Figs. S24, SI). As shown in Fig. 5B-F, IMQ@IONs/ICG + L treatment significantly increased the tumor infiltration of T cells, and decreased the percent-age of Tr_{egs} in the tumors. Immunofluorescence staining also showed higher expression of $CD8^+$ T cells in the tumors treated by IMQ@IONs/ICG + L (Fig. S25). These results indicated that IMQ@IONs/ICG based IPTT-immunotherapy effectively induced the polarization of macrophages to the M1 phenotype, significantly increased the T cell infiltrations, and stimulated cytokine secretion. These effects accordingly induced a systemic immune response *in vivo* and subsequently gave rise to a potent antimetastatic effect. Together, IMQ@IONs/ICG nanoplatform synergizes the ION and ICG to increase the cellular uptake of ION-ICG so that at the low level of light dose the photothermal cytotoxicity can be effective in killing tumor cells while sparing normal cells not containing ION-ICG, the inclusion of IMQ in the platform enhanced the direct immunological stimulation, particularly with the exposure of tumor antigens released by the ION-IGC assisted photothermal effect. Furthermore, to the best of our knowledge, this is the first time that an immunological based nanoplatform like IMQ@IONs/ICG has been used in the interventional light irradiation of orthotopic pancreatic tumors. Since ICG and IMQ have been approved for human use, this innovative nanoplatform hold promise in clinical applications for interventional treatment of metastatic cancers.

4. Conclusion

In conclusion, a coordinated treatment strategy for metastatic PC was developed herein by IPTT-synergized immunotherapy guided by MR imaging and MR temperature monitoring, based on TME-responsive iron oxide nanoparticles loaded with IMQ and ICG (IMQ@IONs/ICG). With a reasonable size of 37.5 nm to enhance nanoparticle accumulation in PC, IMQ@IONs/ICG demonstrated excellent photothermal conversion performance for the efficient destruction of tumors under MR-guided interventional laser irradiation. IPTT induced *in situ* vaccination was amplified by the presence of IMQ, triggering a strong antitumor systemic immunity to control residual tumor cells and metastases which was further enhanced by IONs with modulation of the TME. Thus, the IPTT-synergized immunotherapy strategy proposed in this study can not only improve the therapeutic outcomes but can also promote the clinical development in PC therapy.

Supplementary Material

Refer to Web version on PubMed Central for supplementary material.

Acknowledgments

The authors acknowledge the financial support from the US National Institutes of Health R01 CA205348, S10OD023508, the National Natural Science Foundation of China 61620106016, 61835009, and Guangdong Province Key Area R&D Program 2019B110233004 and Hainan University R&D Program KYQD(ZR)20074, Shenzhen Fundamental Research Program JCYJ20190808114609361.

References

[1]. Kleeff J, Korc M, Apte M, La Vecchia C, Johnson CD, Biankin AV, Neale RE, Tempero M, Tuveson DA, Hruban RH, Neoptolemos JP, Pancreatic cancer, Nat. Rev. Dis. Prim 2 (1) (2016) 16022. [PubMed: 27158978]

[2]. Siegel RL, Miller KD, Jemal A, Cancer statistics, CA-Cancer J. Clin 69 (1) (2019) 7–34. [PubMed: 30620402]

[3]. Rahib L, Smith BD, Aizenberg R, Rosenzweig AB, Fleshman JM, Matrisian LM, Projecting cancer incidence and deaths to 2030: the unexpected burden of thyroid, liver, and pancreas cancers in the United States, Cancer Res. 74 (11) (2014) 2913. [PubMed: 24840647]

[4]. Neoptolemos JP, Kleeff J, Michl P, Costello E, Greenhalf W, Palmer DH, Therapeutic developments in pancreatic cancer: current and future perspectives, Nat. Rev. Gastro. Hepat 15 (6) (2018) 333–348.

[5]. Dolmans DE, Fukumura D, Jain RK, Photodynamic therapy for cancer, Nat. Rev. Cancer 3 (5) (2003) 380–387. [PubMed: 12724736]

[6]. Hu Y, Chi C, Wang S, Wang L, Liang P, Liu F, Shang W, Wang W, Zhang F, Li S, Shen H, Yu X, Liu H, Tian J, A comparative study of clinical intervention and interventional photothermal therapy for pancreatic cancer, Adv. Mater 29 (33) (2017) 1700448.

[7]. Zhou F, Yang J, Zhang Y, Liu M, Lang ML, Li M, Chen WR, Local phototherapy synergizes with immunoadjuvant for treatment of pancreatic cancer through induced immunogenic tumor vaccine, Clin. Cancer Res 24 (21) (2018) 5335–5346. [PubMed: 30068705]

[8]. Chen Q, Chen M, Liu Z, Local biomaterials-assisted cancer immunotherapy to trigger systemic antitumor responses, Chem. Soc. Rev 48 (22) (2019) 5506–5526. [PubMed: 31589233]

[9]. Zhou R, Liu X, Wu Y, Xiang H, Cao J, Li Y, Yin W, Zu Y, Li J, Liu R, Zhao F, Liu Z, Chen C, Gu Z, Yan L, Zhao Y, Suppressing the radiation-induced corrosion of bismuth nanoparticles for enhanced synergistic cancer radiophototherapy, ACS Nano 14 (10) (2020) 13016–13029. [PubMed: 32898419]

[10]. Pardoll DM, Immunology beats cancer: a blueprint for successful translation, Nat. Immunol 13 (12) (2012) 1129–1132. [PubMed: 23160205]

[11]. Couzin-Frankel J, Cancer immunotherapy, Science 342 (6165) (2013) 1432. [PubMed: 24357284]

[12]. Pardoll DM, The blockade of immune checkpoints in cancer immunotherapy, Nat. Rev. Cancer 12 (4) (2012) 252–264. [PubMed: 22437870]

[13]. Postow MA, Callahan MK, Barker CA, Yamada Y, Yuan J, Kitano S, Mu Z, Rasalan T, Adamow M, Ritter E, Sedrak C, Jungbluth AA, Chua R, Yang AS, Roman RA, Rosner S, Benson B, Allison JP, Lesokhin AM, Gnjatic S, Wolchok JD, Immunologic correlates of the abscopal effect in a patient with melanoma, N. Engl. J. Med 366 (10) (2012) 925–931. [PubMed: 22397654]

[14]. Castano AP, Mroz P, Hamblin MR, Photodynamic therapy and anti-tumour immunity, Nat. Rev. Cancer 6 (7) (2006) 535–545. [PubMed: 16794636]

[15]. Ludgate CM, Optimizing cancer treatments to induce an acute immune response: radiation abscopal effects, PAMPs, and DAMPs, Clin. Cancer Res 18 (17) (2012) 4522. [PubMed: 22761465]

[16]. Fan W, Yung B, Huang P, Chen X, Nanotechnology for multimodal synergistic cancer therapy, Chem. Rev 117 (22) (2017) 13566–13638. [PubMed: 29048884]

[17]. Irvine DJ, Hanson MC, Rakhra K, Tokatlian T, Synthetic nanoparticles for vaccines and immunotherapy, Chem. Rev 115 (19) (2015) 11109–11146. [PubMed: 26154342]

[18]. Liang C, Xu L, Song G, Liu Z, Emerging nanomedicine approaches fighting tumor metastasis: animal models, metastasis-targeted drug delivery, phototherapy, and immunotherapy, Chem. Soc. Rev 45 (22) (2016) 6250–6269. [PubMed: 27333329]

[19]. Li Q, Zhang D, Zhang J, Jiang Y, Song A, Li Z, Luan Y, A Three-in-one immunotherapy nanoweapon via cascade-amplifying cancer-immunity cycle against tumor metastasis, relapse, and postsurgical regrowth, Nano Lett. 19 (9) (2019) 6647–6657. [PubMed: 31409072]

[20]. Fang L, Zhao Z, Wang J, Zhang P, Ding Y, Jiang Y, Wang D, Li Y, Engineering autologous tumor cell vaccine to locally mobilize antitumor immunity in tumor surgical bed, Sci. Adv 6 (25) (2020) eaba4024. [PubMed: 32596457]

[21]. Ni K, Lan G, Guo N, Culbert A, Luo T, Wu T, Weichselbaum RR, Lin W, Nanoscale metal-organic frameworks for x-ray activated *in situ* cancer vaccination, Sci. Adv 6 (40) (2020) 5223.

[22]. Zhou Z, Wu H, Yang R, Xu A, Zhang Q, Dong J, Qian C, Sun M, GSH depletion liposome adjuvant for augmenting the photothermal immunotherapy of breast cancer, Sci. Adv 6 (36) (2020) 4373.

[23]. Chen C, Wu Z, Ding P, Sun N, Liu H, Chen Y, Wang Z, Pei R, Peptide NGR modified TiO_2 nanofiber substrate for circulating tumor cells capture, Adv. Fiber Mater 2 (4) (2020) 186–193.

[24]. Wang M, Tan Y, Li D, Xu G, Yin D, Xiao Y, Xu T, Chen X, Zhu X, Shi X, Negative isolation of circulating tumor cells using a microfluidic platform integrated with streptavidin-functionalized PLGA nanofibers, Adv. Fiber Mater 3 (3) (2021) 192–202.

[25]. Zhao J, Cui W, Functional electrospun fibers for local therapy of cancer, Adv. Fiber Mater 2 (5) (2020) 229–245.

[26]. Lv K, Lin H, Qu F, Biodegradable hollow Co_3 S_4@N-doped carbon as enhanced PTT/PDT agent for multimodal MR/thermal imaging and synergistic antitumor therapy, Chem. Eng. J 392 (2020) 124555.

[27]. Wang Y, Zhao J, Chen Z, Zhang F, Wang Q, Guo W, Wang K, Lin H, Qu F, Construct of $MoSe_2/Bi_2Se^3$ nanoheterostructure: multimodal CT/PT imaging-guided PTT/PDT/chemotherapy for cancer treating, Biomaterials 217 (2019) 119282. [PubMed: 31260884]

[28]. Sang D, Wang K, Sun X, Wang Y, Lin H, Jia R, Qu F, NIR-driven intracellular photocatalytic O_2 evolution on Z-scheme $Ni_3S_2/Cu_{1.8}$ S@HA for hypoxic tumor therapy, ACS Appl. Mater. Interfaces 13 (8) (2021) 9604–9619. [PubMed: 33605733]

[29]. Zhou F, Wang M, Luo T, Qu J, Chen WR, Photo-activated chemo-immunotherapy for metastatic cancer using a synergistic graphene nanosystem, Biomaterials 265 (2021) 120421. [PubMed: 32992117]

[30]. Zhao P, Wang M, Chen M, Chen Z, Peng X, Zhou F, Song J, Qu J, Programming cell pyroptosis with biomimetic nanoparticles for solid tumor immunotherapy, Biomaterials 254 (2020) 120142. [PubMed: 32485591]

[31]. Li Y, Jia R, Lin H, Sun X, Qu F, Synthesis of $MoSe_2/CoSe_2$ nanosheets for NIR-enhanced chemodynamic therapy via synergistic *in-situ* H_2O_2 production and activation, Adv. Funct. Mater 31 (8) (2021) 2008420.

[32]. Wang M, Zhou B, Wang L, Zhou F, Smith N, Saunders D, Towner RA, Song J, Qu J, Chen WR, Biodegradable pH-responsive amorphous calcium carbonate nanoparticles as immunoadjuvants for multimodal imaging and enhanced photoimmunotherapy, J. Mater. Chem. B 8 (36) (2020) 8261–8270. [PubMed: 32812632]

[33]. Zhang F, Han X, Hu Y, Wang S, Liu S, Pan X, Wang H, Ma J, Wang W, Li S, Wu Q, Shen H, Yu X, Yuan Q, Liu H, Interventional photothermal therapy enhanced brachytherapy: a new strategy to fight deep pancreatic cancer, Adv. Sci 6 (5) (2019) 1801507.

[34]. Kang S, Gil YG, Min DH, Jang H, Nonrecurring circuit nanozymatic enhancement of hypoxic pancreatic cancer phototherapy using speckled Ru–Te hollow nanorods, ACS Nano 14 (4) (2020) 4383–4394. [PubMed: 32196307]

[35]. Fütterer JJ, Briganti A, De Visschere P, Emberton M, Giannarini G, Kirkham A, Taneja SS, Thoeny H, Villeirs G, Villers A, Can clinically significant prostate cancer be detected with multiparametric magnetic resonance imaging? A systematic review of the literature, Eur. Urol 68 (6) (2015) 1045–1053. [PubMed: 25656808]

[36]. Magnetic Resonance Imaging, Visual guide to neonatal cardiology 2018, pp. 104–108.

[37]. Poorter JD, Noninvasive MRI thermometry with the proton resonance frequency method: study of susceptibility effects, Magn. Reson. Med 34 (3) (1995) 359–367. [PubMed: 7500875]

[38]. Quesson B, de Zwart JA, Moonen CTW, Magnetic resonance temperature imaging for guidance of thermotherapy, J. Magn. Reson. Imaging 12 (4) (2000) 525–533. [PubMed: 11042633]

[39]. Rieke V, Butts Pauly K, MR thermometry, J. Magn. Reson. Imaging 27 (2) (2008) 376–390. [PubMed: 18219673]

[40]. Todd N, Diakite M, Payne A, Parker DL, *In vivo* evaluation of multi-echo hybrid PRF/T1 approach for temperature monitoring during breast MR-guided focused ultrasound surgery treatments, Magn. Reson. Med 72 (3) (2014) 793–799. [PubMed: 24259398]

[41]. Winter L, Oberacker E, Paul K, Ji Y, Oezerdem C, Ghadjar P, Thieme A, Budach V, Wust P, Niendorf T, Magnetic resonance thermometry: methodology, pitfalls and practical solutions, Int. J. Hyperther 32 (1) (2016) 63–75.

[42]. Zhu M, Sun Z, Ng CK, Image-guided thermal ablation with MR-based thermometry, Quant. Imag. Med. Surg 7 (3) (2017) 356–368.

[43]. Asadi M, Beik J, Hashemian R, Laurent S, Farashahi A, Mobini M, Ghaznavi H, Shakeri-Zadeh A, MRI-based numerical modeling strategy for simulation and treatment planning of nanoparticle-assisted photothermal therapy, Phys. Med 66 (2019) 124–132. [PubMed: 31600672]

[44]. Farashahi A, Zare-Sadeghi A, Shakeri-Zadeh A, Kamran Kamrava S, Maleki S, Ghaznavi H, Faeghi F, Real-time mapping of heat generation and distribution in a laser irradiated agar phantom loaded with gold nanoparticles using MR temperature imaging, Photodiagn. Photodyn 25 (2019) 66–73.

[45]. Gallo J, Long NJ, Aboagye EO, Magnetic nanoparticles as contrast agents in the diagnosis and treatment of cancer, Chem. Soc. Rev 42 (19) (2013) 7816–7833. [PubMed: 23788179]

[46]. Lee N, Yoo D, Ling D, Cho MH, Hyeon T, Cheon J, Iron oxide based nanoparticles for multimodal imaging and magnetoresponsive therapy, Chem. Rev 115 (2015) 10637–10689. [PubMed: 26250431]

[47]. Lu Y, Xu YJ, Zhang GB, Ling D, Wang MQ, Zhou Y, Wu YD, Wu T, Hackett MJ, Hyo Kim B, Chang H, Kim J, Hu XT, Dong L, Lee N, Li F, He JC, Zhang L, Wen HQ, Yang B, Hong Choi S, Hyeon T, Zou DH, Iron oxide nanoclusters for T1 magnetic resonance imaging of non-human primates, Nat. Biomed. Eng 1 (8) (2017) 637–643. [PubMed: 31015599]

[48]. Lee N, Hyeon T, Designed synthesis of uniformly sized iron oxide nanoparticles for efficient magnetic resonance imaging contrast agents, Chem. Soc. Rev 41 (7) (2012) 2575–2589. [PubMed: 22138852]

[49]. Min Y, Caster JM, Eblan MJ, Wang AZ, Clinical translation of nanomedicine, Chem. Rev 115 (19) (2015) 11147–11190. [PubMed: 26088284]

[50]. Zanganeh S, Hutter G, Spitler R, Lenkov O, Mahmoudi M, Shaw A, Pajarinen JS, Nejadnik H, Goodman S, Moseley M, Coussens LM, Daldrup-Link HE, Iron oxide nanoparticles inhibit tumour growth by inducing pro-inflammatory macrophage polarization in tumour tissues, Nat. Nanotechnol 11 (2016) 986. [PubMed: 27668795]

[51]. Li M, Lin H, Qu F, FeS_2@C-ICG-PEG nanostructure with intracellular O_2 generation for enhanced photo-dynamic/thermal therapy and imaging, Chem. Eng. J 384 (2020) 123374.

[52]. Tang Z, Zhao P, Wang H, Liu Y, Bu W, Biomedicine meets Fenton chemistry, Chem. Rev 121 (4) (2021) 1981–2019. [PubMed: 33492935]

[53]. Beik J, Asadi M, Khoei S, Laurent S, Abed Z, Mirrahimi M, Farashahi A, Hashemian R, Ghaznavi H, Shakeri-Zadeh A, Simulation-guided photothermal therapy using MRI-traceable iron oxide-gold nanoparticle, J. Photochem. Photobiol. B Biol 199 (2019) 111599.

[54]. Erkan M, Hausmann S, Michalski CW, Fingerle AA, Dobritz M, Kleeff J, Friess H, The role of stroma in pancreatic cancer: diagnostic and therapeutic implications, Nat. Rev. Gastroenterol. Hepatol 9 (8) (2012) 454–467. [PubMed: 22710569]

[55]. Neesse A, Bauer CA, Ohlund D, Lauth M, Buchholz M, Michl P, Tuveson DA, Gress TM, Stromal biology and therapy in pancreatic cancer: ready for clinical translation? Gut 68 (1) (2019) 159–171. [PubMed: 30177543]

[56]. Wilhelm S, Tavares AJ, Dai Q, Ohta S, Audet J, Dvorak HF, Chan WCW, Analysis of nanoparticle delivery to tumours, Nat. Rev. Mater 1 (5) (2016) 16014.

[57]. Buchold DHM, Feldmann C, Nanoscale γ-AlO(OH) hollow spheres: synthesis and container-type functionality, Nano Lett. 7 (11) (2007) 3489–3492. [PubMed: 17958390]

[58]. Li M, Zhang Y, Liu Z, Bharadwaj U, Wang H, Wang X, Zhang S, Liuzzi JP, Chang SM, Cousins RJ, Fisher WE, Brunicardi FC, Logsdon CD, Chen C, Yao Q, Aberrant expression of zinc transporter ZIP4 (SLC39A4) significantly contributes to human pancreatic cancer pathogenesis and progression, Proc. Natl. Acad. Sci. U.S.A 104 (47) (2007) 18636. [PubMed: 18003899]

[59]. Li M, Zhang Y, Bharadwaj U, Zhai Q, Ahern CH, Fisher WE, Brunicardi FC, Logsdon CD, Chen C, Yao Q, Down-regulation of ZIP4 by RNA interference inhibits pancreatic cancer growth and increases the survival of nude mice with pancreatic cancer xenografts, Clin. Cancer Res 15 (19) (2009) 5993. [PubMed: 19755388]

[60]. Chen Y, Gnyawali SC, Wu F, Liu H, Tesiram YA, Abbott A, Towner RA, Chen WR, Magnetic resonance imaging guidance for laser photothermal therapy, J. Biomed. Opt 13 (4) (2008) 044033. [PubMed: 19021360]

[61]. Le K, Li X, Figueroa D, Towner RA, Garteiser P, Saunders D, Smith N, Liu H, Hode T, Nordquist RE, Chen WR, Assessment of thermal effects of interstitial laser phototherapy on mammary tumors using proton resonance frequency method, J. Biomed. Opt 16 (12) (2011) 128001. [PubMed: 22191937]

[62]. Liu S, Doughty A, West C, Tang Z, Zhou F, Chen WR, Determination of temperature distribution in tissue for interstitial cancer photothermal therapy, Int. J. Hyperth 34 (6) (2018) 756–763.

Statement of significance

Pancreatic cancer (PC) is one of the most lethal malignancies because it is non-permeable to drugs and highly metastatic. In this study, we designed a tumor microenvironment-responsive amorphous iron oxide nanoplatform (ION) to co-deliver photothermal agent (ICG) and toll-like-receptor-7 agonist (IMQ). This biodegradable nanoplatform IMQ@IONs/ICG improved the penetration of the loaded drugs in pancreatic tumor. With MR imaging guidance and temperature monitoring, the precise interventional photothermal therapy on mouse Panc02-H7 orthotopic tumors releases tumor antigens to initiate tumor-special immune responses, amplified by the released IMQ. Our results demonstrate that IMQ@IONs/ICG overcomes the obstacle of drug delivery to pancreatic tumors, and when combined with photothermal therapy, induces a systemic antitumor immunity to control metastatic tumors.

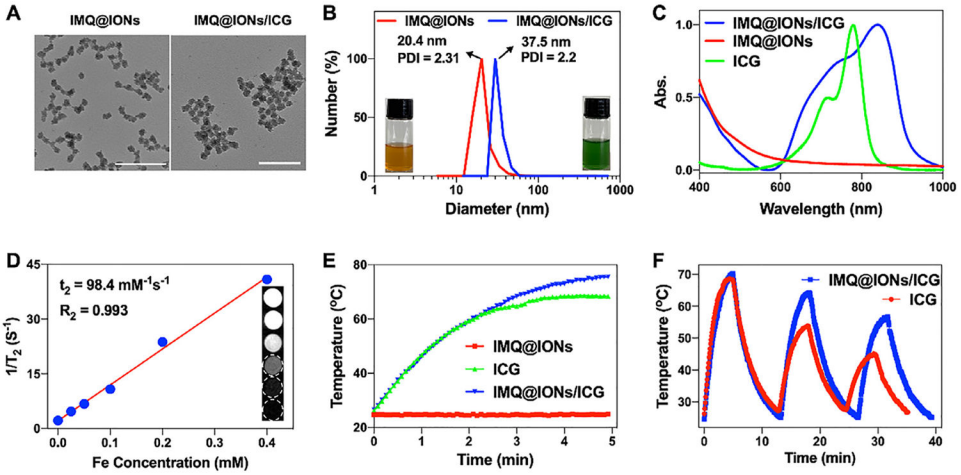

Fig. 1.

Characterization of IMQ@IONs/ICG. (A) TEM images of IMQ@IONs and IMQ@IONs/ICG. Scale bar = 100 nm. (B) Size distribution of IMQ@IONs and IMQ@IONs/ICG (Insets: Photographs of IMQ@IONs and IMQ@IONs/ICG dispersed in aqueous solution). (C) Vis–NIR absorbance spectra of ICG, IMQ@IONs, and IMQ@IONs/ICG. (D) T_2 relaxation rate ($1/T_2$) of IMQ@IONs/ICG (Inset: T_2-weighted MR images of IMQ@IONs/ICG). (E) Temperature elevations of IMQ@IONs, ICG, and IMQ@IONs/ICG under 805 nm laser irradiation (0.75 W cm^{-2}, 5 min). (F) Temperature elevations of ICG and IMQ@IONs/ICG under 805 nm laser irradiation for 3 irradiation-relaxation cycles.

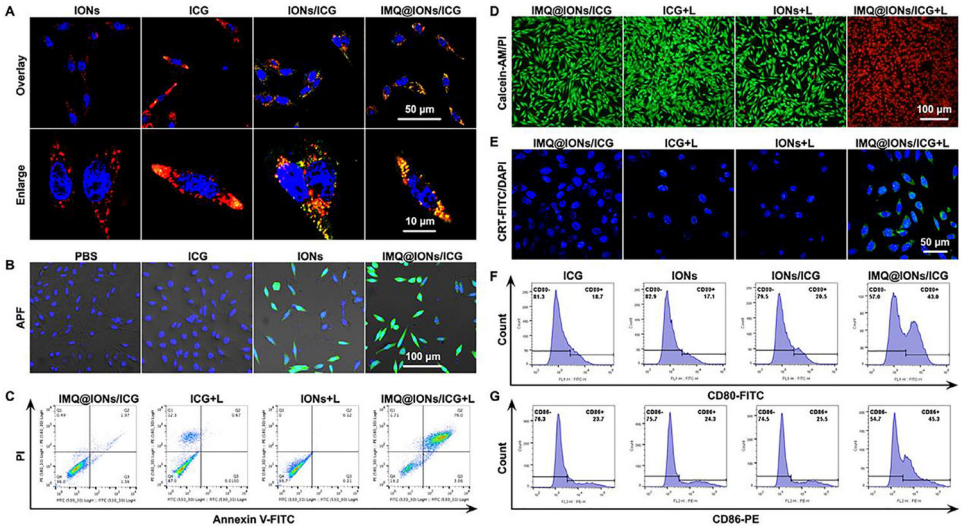

Fig. 2.

Cellular study of IMQ@IONs/ICG with or without laser irradiation. (A) Representative fluorescence images of Panc02-H7 cells showing intracellular uptake of nanoparticles. Blue: DAPI, Red: Lyso-tracker, Green: ICG. (B) Representative fluorescence images of Panc02-H7 cells showing intracellular production of •OH (green) induced by nanoparticles. Blue: DAPI, Green: APF. (C, D) Representative flow scatter plot and fluorescence images showing cell death of Panc02-H7 cells after treatment with IMQ@IONs/ICG plus laser irradiation (0.75 W cm $^{-2}$, 5 min), with Annexin V-FITC/PI staining (C) or Calcein-AM/PI staining (D). (E) Representative fluorescence images of Panc02-H7 cells showing CRT exposure on the surface after treatment with IMQ@IONs/ICG plus laser irradiation. (F, G) Representative flow graph showing CD80 and CD86 expressions on the surface of DCs stimulated by different nanoparticles.

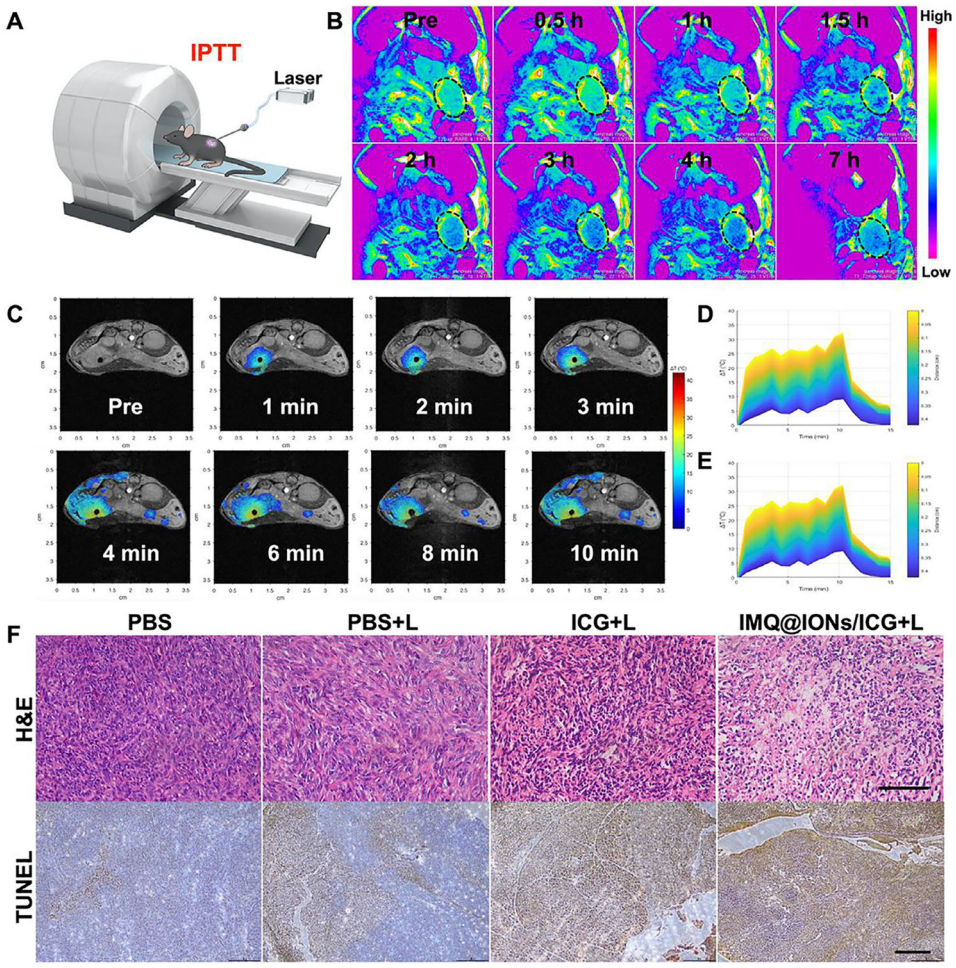

Fig. 3.

In vivo MR imaging guided interventional photothermal therapy (IPTT) with IMQ@IONs/ICG. (A) Schematic depiction of IPTT guided by MRI. (B) MR images of Panc02-H7 tumor-bearing mice at different times after intravenous injection of IMQ@IONs/ICG nanoparticles. (C) MR images showing temperature distribution in pancreatic tumor during IPTT treatment. (D, E) Temperature increase curves in tumor based on MR imaging data (D) and IR thermal imaging data (E). (F) Histology images of excised tumors after treatment. Upper row shows H&E staining, scale bar = 100 μm; lower row shows TUNEL staining, scale bar = 200 μm.

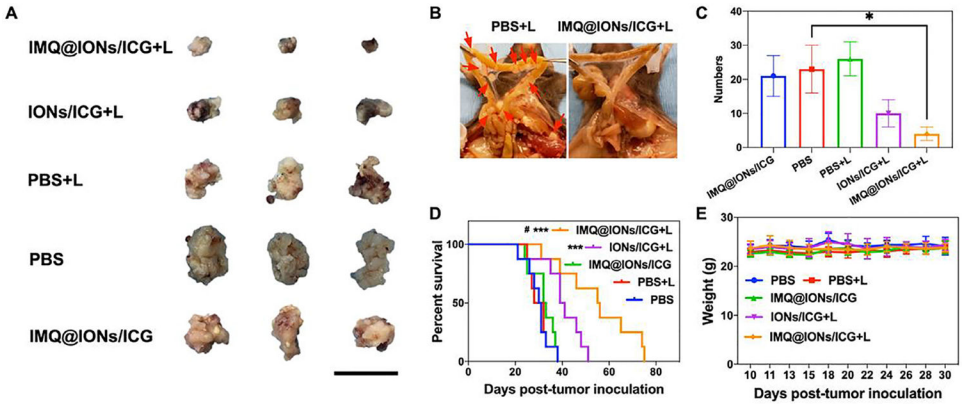

Fig. 4.

Therapeutic effects of IMQ@IONs/ICG on Panc02-H7 orthotopic PC. (A) Photographs of the primary tumors 7 days after different treatments. Scale bar = 2 cm. (B) Representative photographs of mesentery metastases 7 days after IMQ@IONs/ICG + L treatments. (C) Numbers of mesentery metastases 7 days after different treatments. (* $p < 0.05$, vs PBS group, $n = 3$, one-way analysis of variance (ANOVA) with Tukey test) (D) Survival rates of Panc02-H7 orthotopic tumor-bearing mice after various treatments. (*** $p < 0.001$, vs PBS group, $^{\#}p < 0.05$, vs IONs/ICG + L, $n = 8$, two-tailed Mantel–Cox test). (E) Average body weight variation of Panc02-H7 orthotopic tumor-bearing mice after various treatments ($n = 8$). Data are expressed as mean ± SD.

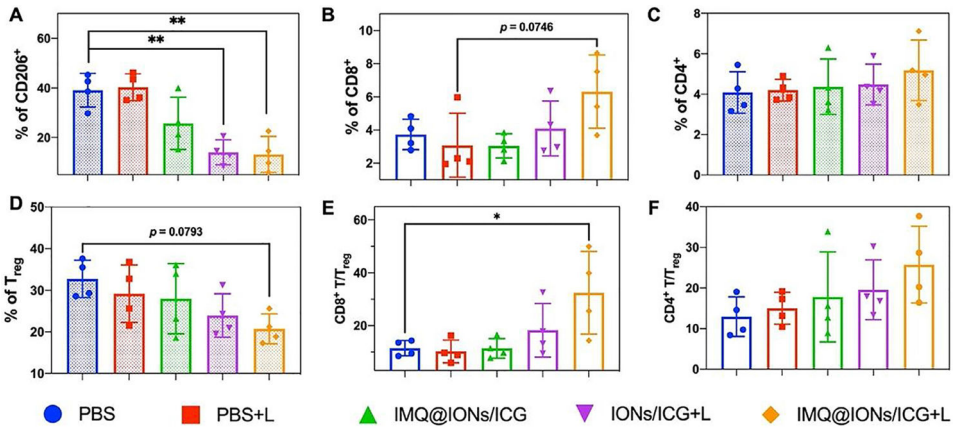

Fig. 5.

Antitumor immunity of IPIT on Panc02-H7 orthotopic PC with IMQ@IONs/ICG. (A) Relative abundance of TAM subpopulation in the tumors 1 day after treatments. TAMs were defined as being $CD205^+F4/80^+$ (** $p < 0.01$, vs PBS group, $n = 4$, one-way ANOVA with Tukey test). (B–F) The relative abundance of $CD8^+$ T-cell, $CD4^+$ T-cell, and T_{reg} subpopulations in tumors 5 days after treatments. T cells were defined as being $CD45^+$, T_{regs} were defined as being $CD45^+CD3^+CD4^+CD25^+FOXP3^+$ (* $p < 0.05$, vs PBS group, $n = 4$, one-way ANOVA with Tukey test). The abundance of immune cells was analyzed by flow cytometry with indicated antibody staining. Data are expressed as mean ± SD.

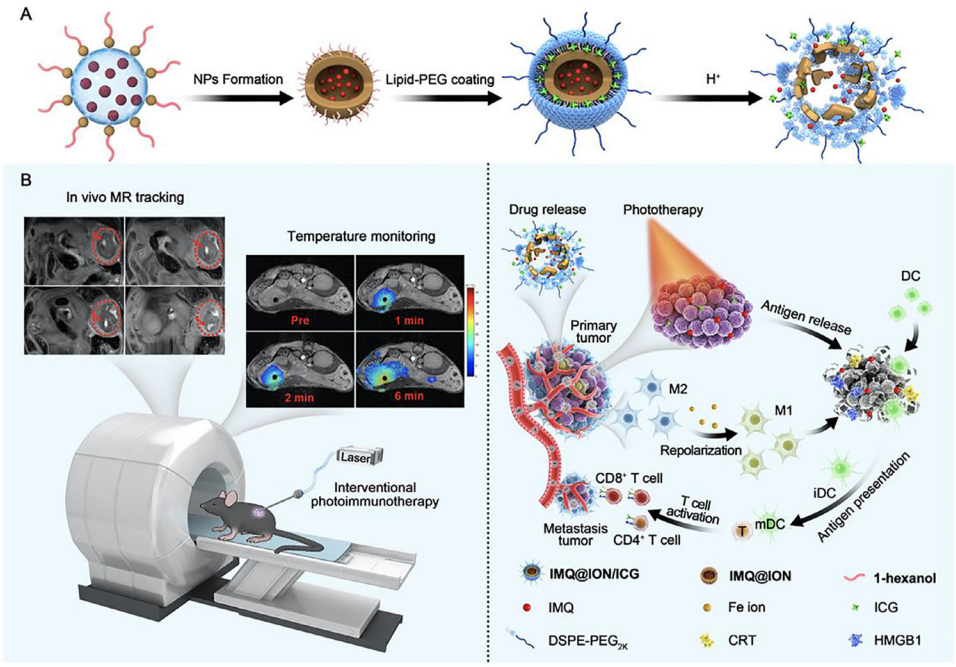

Scheme 1.

Schematic illustration of IMQ@IONs/ICG-mediated interventional photothermal-immunotherapy for the treatment of metastatic pancreatic cancer. (A) Preparation process of the IMQ@IONs/ICG nanoplatform. (B) Left: schematic diagram of interventional photothermal-immunotherapy with imaging guidance and temperature monitoring by magnetic resonance (MR) technique. Right: mechanism of anti-tumor immune response induced by IMQ@IONs/ICG based interventional photothermal-immunotherapy.